Supporting information for:

Signatures of solvation thermodynamics in spectra of intermolecular vibrations

Rasmus A. X. Persson,[†] Viren Pattni,[†] Anurag Singh,[†,‡] Stefan M. Kast,[¶] and Matthias Heyden[*,†]

Max-Planck-Institut für Kohlenforschung, Kaiser-Wilhelm-Platz 1, DE-45470 Mülheim an der Ruhr, Germany, Department of Chemistry, Indian Institute of Technology, Roorkee, IN-247667 Roorkee, Uttarakhand, India, and Physikalische Chemie III, Technische Universität Dortmund, Otto-Hahn-Straße 4a, DE-44227 Dortmund, Germany

E-mail: heyden@kofo.mpg.de

Phone: +49 208 306 2162. Fax: +49 208 306 2996

---

[*]To whom correspondence should be addressed

[†]Max-Planck-Institut für Kohlenforschung, Kaiser-Wilhelm-Platz 1, DE-45470 Mülheim an der Ruhr, Germany

[‡]Department of Chemistry, Indian Institute of Technology, Roorkee, IN-247667 Roorkee, Uttarakhand, India

[¶]Physikalische Chemie III, Technische Universität Dortmund, Otto-Hahn-Straße 4a, DE-44227 Dortmund, Germany

Solvation free energies from thermodynamic integration

Total solvation free energies, without decompositions into enthalpic and entropic components or local contributions, can be obtained from thermodynamic integration simulations. For each of the systems studied in this work, we obtained the free energy difference between a system with a fully decoupled solute ($\lambda = 0$, i.e. no interactions between the solute and the solvent) and a fully coupled solute ($\lambda = 1$, i.e. solute-solvent interactions are switched on). For solutes carrying atoms with non-zero charges, we carried out these simulations in two distinct stages: 1) one set of simulations in which the Lennard-Jones interactions between the solute and solvent were smoothly switched on using a soft-core potential and 2) one subsequent set of simulations in which the electrostatic interactions between the solute and the solvent were switched on. For the neutral rare gas atoms, the second stage was omitted due to absence of electrostatic interactions between the solute and the solvent. Simulations were started from an equilibrated structure obtained from the 3D-2PT simulations with a fully coupled solute. Each thermodynamic integration stage described above included simulations for 21 distinct values for the parameter λ between 0 and 1. The intervals between λ-values were chosen to minimize the statistical error obtained for the total free energy. Simulations for each λ value were carried out for 1 ns of which the first 100 ps were disregarded to allow for equilibration. A stochastic dynamics integrator was employed with a time step of 2 fs. These simulations were carried out in the isothermal-isobaric ensemble using the Nose-Hoover thermostat[S1] and the Parrinello-Rahman barostat[S2] at 300K and 1 bar with time constants of 0.5 and 5.0 ps, respectively. All other simulation parameters were identical to the 3D-2PT simulations, including fixed solute coordinates. All simulations were carried out using the Gromacs 4.6.1 software[S3] and analyzed with the built-in 'g_bar' tool utilizing Bennett's acceptance ratio (BAR) to obtain free energy differences between the simulated states.[S4] The results are shown below in Table S1 in comparison to results obtained from the 3D-2PT approach via $\Delta U_{\text{solv}} - T\Delta S_{\text{solv}}$ (see Table S2) and experimental data.[S5–S7] The RMSD between the 3D-2PT data and the experimental solvation free energies is 8.4 kJ mol^{-1}. The solvation free energies obtained directly from thermodynamic integration have an RMSD of 4.6 kJ mol^{-1} relative to the experimental data, indicating

the accuracy limit determined by the employed force field parameters.

Table S1: Solvation free energies $\Delta G_{\text{solv}} = \Delta H_{\text{solv}} - T\Delta S_{\text{solv}}$ obtained with the 3D-2PT method for atomic, ionic and molecular solutes in water at 300K in comparison to thermodynamic integration simulations (MD-TI) and experimental data. [a]exp. data from Ref. S5; [b]exp. data from Ref. S6; [c]exp. data from Ref. S7. All values for ΔG_{solv} are given in kJ/mol.

	3D-2PT	MD-TI	exp.
[a]F^-	-520.9±4.6	-499.5±0.5	-500.8
[a]Cl^-	-376.0±4.9	-374.3±0.9	-372.7
[a]Br^-	-354.3±5.9	-345.7±0.9	-346.4
[a]I^-	-321.6±4.9	-310.9±0.8	-311.8
[a]Na^+	-366.6±6.3	-371.8±0.4	-370.5
[a]K^+	-288.0±5.3	-295.8±0.4	-298.3
[b]Neon	+7.9±1.4	+11.6±0.3	+11.3
[b]Argon	+1.5±1.6	+8.8±0.3	+8.5
[b]Xenon	-0.9±1.1	-7.7±0.5	+5.7
[c]Methanol	-22.8±1.9	-21.4±0.8	-21.2
[c]Benzene	-9.5±2.1	-3.2±0.3	-3.5
[c]NMA	-44.2±1.9	-33.9±0.7	-41.9

Cut-off corrections for the solvation enthalpy of charged solutes

The local contributions to the solvation enthalpy described in Eq. 1 of the main text are computed based on a real-space cut-off. Therefore, long-ranged electrostatic interactions and interactions with a uniform counter-charge, introduced for non-neutral systems by the particle mesh Ewald summation method employed during the simulation, are not taken into account. We note that the ion force field parameters used here[S8] were optimized to reproduce experimental solvation free energies in simulations employing an Ewald summation procedure. The interaction of a single charge with a uniformly distributed counter-charge is non-negligible and can amount to -110 kJ mol^{-1} for systems of the size considered here. The correction for each system is estimated here by extending simulations of the fully decoupled and the fully coupled system, as obtained above for the thermo-dynamic integration calculations, to a total length of 10 ns. The systems total energy was computed every 100 fs, taking long-ranged interactions and interactions with the uniform counter-charge into account. An estimate of the solvation enthalpy, $\Delta H_{\text{solv}}^{\text{PME}}$, can then be obtained from the difference

of the average total energy of the coupled and decoupled system. The energies in both stored trajectories were then recomputed using the same cut-off definition as in the calculation of local solvation enthalpy contributions within 3D-2PT. The difference between the average total energy of the coupled and decoupled system, $\Delta H_{\text{solv}}^{\text{cutoff}}$, obtained this way, allows us to obtain a correction for the total solvation enthalpy obtained from summing over the local contributions in Eq. 2 in the main text as $\Delta H_{\text{solv}}^{\text{corr}} = \Delta H_{\text{solv}}^{\text{PME}} - \Delta H_{\text{solv}}^{\text{cutoff}}$. This correction is only significant for charged solutes. Due to the less pronounced sampling used to compute this correction, it increases the statistical uncertainty. Hence, we apply the correction only for the charged systems, where the correction is larger than its associated uncertainty.

Table S2: Solvation enthalpies (ΔH_{solv}) and entropies ($-T\Delta S_{\text{solv}}$) obtained with the 3D-2PT method for atomic, ionic and molecular solutes in water at 300K in comparison to experimental data and a previous GCT study as shown in Fig. 3. [a]exp. data from Ref. S5; [b]exp. data from Ref. S6; [c]exp. data from Ref. S7; [d]GCT data from Ref. S7. All vaules for ΔH_{solv} and $-T\Delta S_{\text{solv}}$ are given in kJ mol^{-1}.

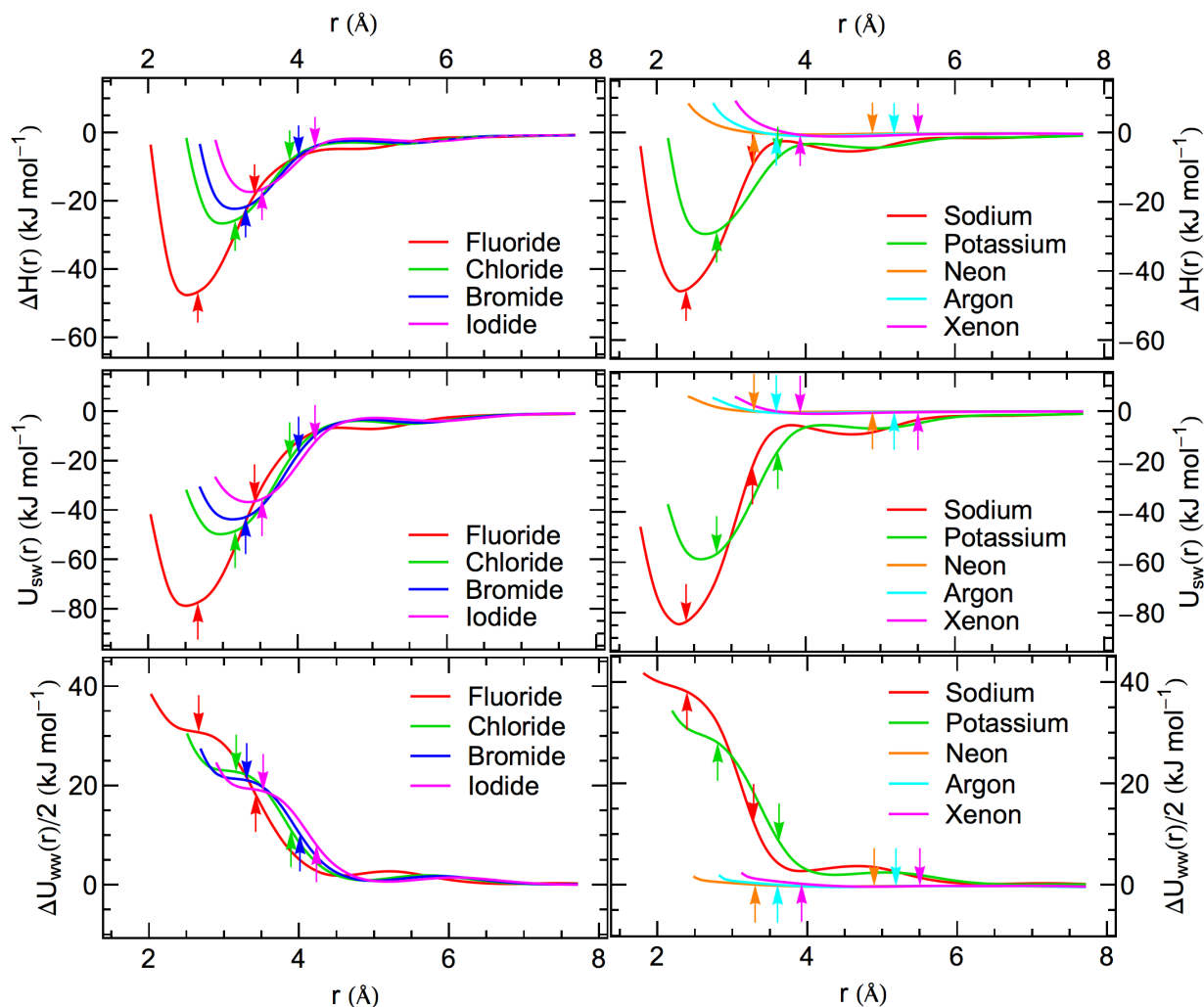|	ΔH_{solv}			$-T\Delta S_{\text{solv}}$		
	3D-2PT	[d]GCT	exp.	3D-2PT	[d]GCT	exp.
[a]F$^-$	-557.3±4.2	–	-539	+36.5±0.4	–	+38.16
[a]Cl$^-$	-391.9±4.6	-286.0±0.6	-392	+15.9±0.3	+13.0±0.7	+19.35
[a]Br$^-$	-364.4±5.1	–	-361	+10.0±0.8	–	+14.61
[a]I$^-$	-324.5±4.1	–	-321	+2.9±0.8	–	+9.18
[a]Na$^+$	-394.2±5.5	-308.0±1.2	-391	+27.6±0.7	+17.9±1.7	+20.49
[a]K$^+$	-302.7±5.1	–	-308	+14.7±0.2	–	+9.66
[b]Neon	-0.2±1.0	+2.6±1.4	-1.44	+8.2±0.5	+6.0±1.6	+12.71
[b]Argon	-10.5±1.1	–	-9.97	+12.0±0.5	–	+18.47
[b]Xenon	-15.2±0.8	-10.0±1.5	-16.12	+14.2±0.3	+12.8±0.7	+21.85
[c]Methanol	-42.7±0.7	-35.7±0.8	-42.01	+20.0±1.2	+21.3±0.3	+20.82
[c]Benzene	-32.6±1.2	-30.5±1.8	-29.29	+23.1±0.9	+27.5±0.3	+25.83
[c]NMA	-72.6±0.9	-71.5±0.4	-73.68	+28.4±1.0	+32.5±1.1	+31.77

Figure S1: Radially resolved contributions to the solvation enthalpy of monoatomic solutes in water. Shown are radial profiles of local solvation enthalpy contributions $\Delta H(r) = U_{sw}(r) + \Delta U_{ww}(r)/2$ (top panels), solute-water interaction energies $U_{sw}(r)$ (mid panels) and deviations of water-water interactions from the bulk average (divided by 2 to avoid double counting in Eq. 2 in the main text) $\Delta U_{ww}(r)/2 = \left[U_{ww}(r) - U_{ww}^{bulk} \right]/2$ (bottom panels). Results are shown for simulations of halide anions (left panels) and sodium and rare gas atoms (right panels). Arrows indicate the position of the first hydration shell (maximum of the $g(r)$) and interstitial water molecules (minimum of the $g(r)$) as in Fig. 4 of the main text. Energies are reported up to a minimum distance for which the corresponding $g(r)$ falls below a value of 0.2, i.e. the potential of mean force becomes strongly repulsive.
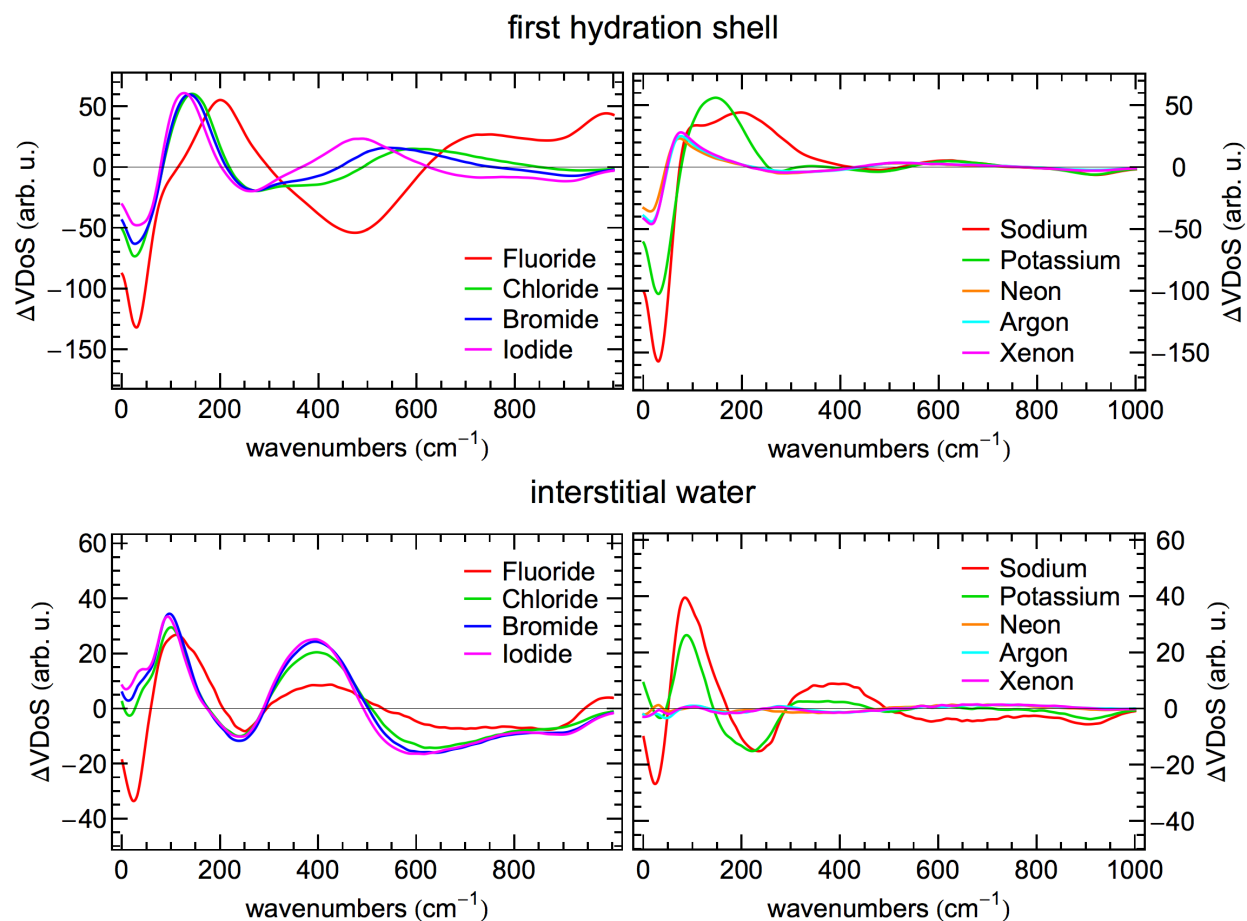
Figure S2: Deviation from the bulk water VDoS for water molecules in the hydration environment of monoatomic solutes: Halide anions (left panels) and alkali cations and rare gas atoms (right panels) as in Fig. 6 of the main text. Results are shown for water molecules in the first hydration shell (top panels) and interstitial waters between the first and second hydration shell (bottom panels), i.e. at distances corresponding to the first maximum and minimum of the respective $g(r)$.
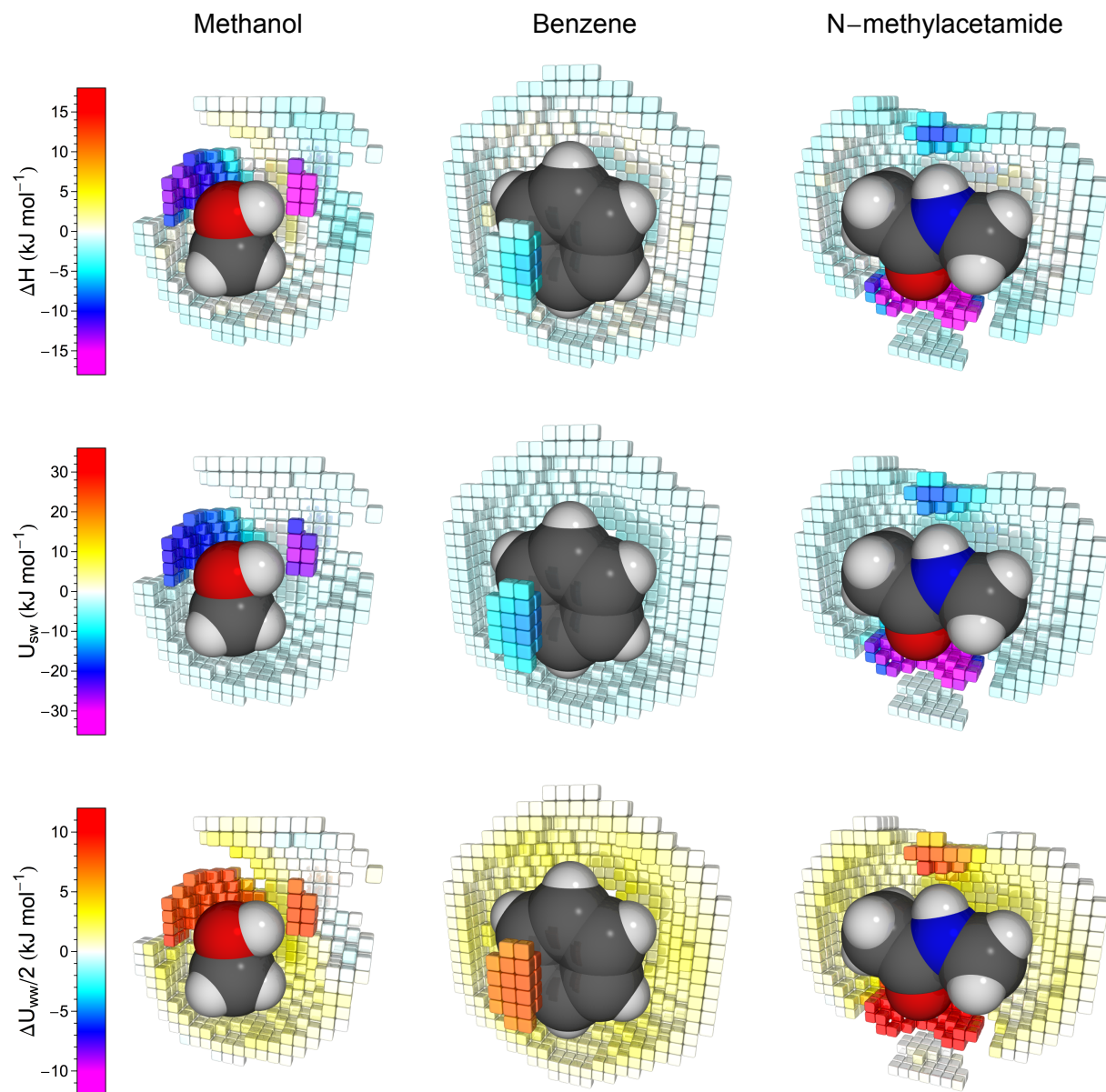
Figure S3: Spatially resolved contributions to the solvation enthalpy in water in the environment of molecular solutes. Shown voxels represent the first hydration shell as in Fig. 7 of the main text, the color code shows local solvation enthalpy contributions $\Delta H(\mathbf{r}) = U_{\mathrm{sw}}(\mathbf{r}) + \Delta U_{\mathrm{ww}}(\mathbf{r})/2$ (top panels), solute-water interaction energies $U_{\mathrm{sw}}(\mathbf{r})$ (mid panels) and deviations of water-water interactions from the bulk average (divided by 2 to avoid double counting in Eq. 2 in the main text) $\Delta U_{\mathrm{ww}}(\mathbf{r})/2 = \left[U_{\mathrm{ww}}(\mathbf{r}) - U_{\mathrm{ww}}^{\mathrm{bulk}} \right]/2$ (bottom panels) according to the corresponding color scale.
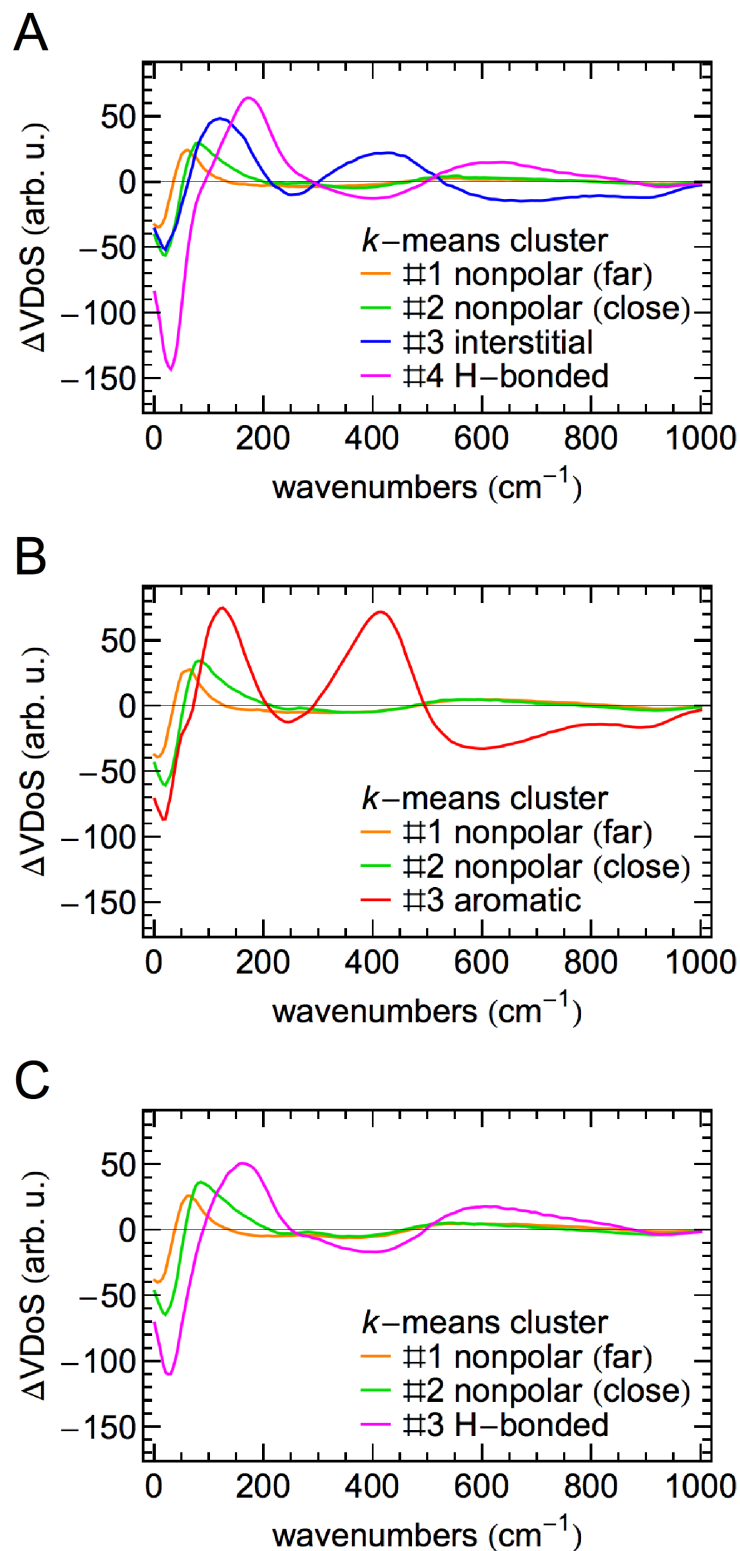
Figure S4: Deviation from the bulk water VDoS for distinct hydration water species obtained from k-means clustering in the hydration shell of molecular solutes in accordance to Fig. 8 in the main text. Results are shown for methanol (A), benzene (B) and N-methylacetamide (C).

References

(S1) Hoover, W.-G. Canonical dynamics: Equilibrium phase-space distributions. *Phys. Rev. A* **1985**, *31*, 1695–1697.

(S2) Parrinello, M.; Rahman, A. Polymorphic transitions in single crystals: A new molecular dynamics method. *J. Appl. Phys.* **1981**, *52*, 7182–7190.

(S3) Hess, B.; Kutzner, C.; van der Spoel, D.; Lindahl, E. GROMACS 4: Algorithms for highly efficient, load-balanced, and scalable molecular simulation. *J. Chem. Theory Comput.* **2008**, *4*, 435–447.

(S4) Bennett, C. H. Efficient estimation of free energy differences from Monte Carlo data. *J. Comp. Phys.* **1976**, *22*, 245–268.

(S5) Schmid, R.; Miah, A. M.; Sapunov, V. N. A new table of the thermodynamic quantities of ionic hydration: values and some applications (enthalpy–entropy compensation and Born radii). *Phys. Chem. Chem. Phys.* **2000**, *2*, 97–102.

(S6) Ben-Naim, A.; Marcus, Y. Solvation thermodynamics of nonionic solutes. *J. Chem. Phys.* **1984**, *81*, 2016–2027.

(S7) Gerogiokas, G.; Calabro, G.; Henchman, R. H.; Southey, M. W.; Law, R. J.; Michel, J. Prediction of small molecule hydration thermodynamics with grid cell theory. *J. Chem. Theory Comput.* **2013**, *10*, 35–48.

(S8) Joung, I. S.; Cheatham III, T. E. Determination of alkali and halide monovalent ion parameters for use in explicitly solvated biomolecular simulations. *J. Phys. Chem. B* **2008**, *112*, 9020–9041.